

Faculty of Medicine  
Biomedical Engineering

Master of Science Thesis

# Intraoperative 3D ultrasound-based planning for surgical resection of liver tumors

by

**Luca Sahli**

of Wohlen b. Bern, Switzerland

Supervisors  
MSc Iwan Paolucci and Prof. Dr.-Ing. Stefan Weber

Institutions  
ARTORG Center for Biomedical Engineering Research, University of Bern

Examiners  
Prof. Dr.-Ing. Stefan Weber and MSc Iwan Paolucci

Bern, October 2018



## Abstract

*The abstract should provide a concise (300-400 word) summary of the motivation, methodology, main results and conclusions. For example:*

Osteoporosis is a disease in which the density and quality of bone are reduced. As the bones become more porous and fragile, the risk of fracture is greatly increased. The loss of bone occurs progressively, often there are no symptoms until the first fracture occurs. Nowadays as many women are dying from osteoporosis as from breast cancer. Moreover it has been estimated that yearly costs arising from osteoporotic fractures alone in Europe worth 30 billion Euros.

Percutaneous vertebroplasty is the injection of bone cement into the vertebral body in order to relieve pain and stabilize fractured and/or osteoporotic vertebrae with immediate improvement of the symptoms. Treatment risks and complications include those related to needle placement, infection, bleeding and cement extravasation. The cement can leak into extraosseous tissues, including the epidural or paravertebral venous system eventually ending in pulmonary embolism and death.

The aim of this project was to develop a computational model to simulate the flow of two immiscible fluids through porous trabecular bone in order to predict the three-dimensional spreading patterns developing from the cement injection and minimize the risk of cement extravasation while maximizing the mechanical effect. The computational model estimates region specific porosity and anisotropic permeability from Hounsfield unit values obtained from patient-specific clinical computer tomography data sets. The creeping flow through the porous matrix is governed by a modified version of Darcy's Law, an empirical relation of the pressure gradient to the flow velocity with consideration of the complex rheological properties of bone cement.

To simulate the immiscible two phase fluid flow, i.e. the displacement of a biofluid by a biomaterial, a fluid interface tracking algorithm with mixed boundary representation has been developed. The nonlinear partial differential equation arising from the problem was numerically implemented into the open-source Finite Element framework *libMesh*. The algorithm design allows the incorporation of the developed methods into a larger simulation of vertebral bone augmentation for pre-surgical planning.

First simulation trials showed close agreement with the findings from relevant literature. The computational model demonstrated efficiency and numerical stability. The future model development may incorporate the morphology of the region specific trabecular bone structure improving the models' accuracy or the prediction of the orientation and alignment of fiber-reinforced bone cements in order to increase fracture-resistance.



## Acknowledgements

*Here you may include acknowledgements.*

*Ich erkläre hiermit, dass ich diese Arbeit selbständig verfasst und keine anderen als die angegebenen Hilfsmittel benutzt habe. Alle Stellen, die wörtlich oder sinngemäss aus Quellen entnommen wurden, habe ich als solche kenntlich gemacht. Mir ist bekannt, dass andernfalls der Senat gemäss dem Gesetz über die Universität zum Entzug des auf Grund dieser Arbeit verliehenen Titels berechtigt ist.*

Bern, October 31<sup>th</sup> 2018

Luca Sahli

# Contents

<b>Contents</b>	<b>vii</b>
<b>1 Introduction</b>	<b>1</b>
1.1 Motivation . . . . .	1
1.2 The Liver . . . . .	1
1.2.1 Liver Anatomy . . . . .	1
1.2.2 Liver Cancer . . . . .	2
1.3 Liver Resections . . . . .	2
1.3.1 Parenchymal-sparing liver surgeries . . . . .	3
1.4 Objectives . . . . .	3
<b>2 State of the art</b>	<b>5</b>
2.1 Intraoperative ultrasound . . . . .	5
2.2 Navigation for liver resections . . . . .	6
2.2.1 Creation of preoperative 3D-models . . . . .	6
2.2.2 Registration methods . . . . .	6
2.2.3 Tracking modalities . . . . .	6
2.3 Surface reconstruction of unorganized points . . . . .	7
2.3.1 Data acquisition . . . . .	7
2.3.2 Reconstruction algorithms . . . . .	7
<b>3 Problem Statement</b>	<b>9</b>
<b>4 Concept</b>	<b>11</b>
4.1 System . . . . .	11
4.2 Functionalities . . . . .	11
4.2.1 Surface Reconstruction . . . . .	12
4.2.2 Tumor Segmentation . . . . .	12
4.2.3 Resection Planning . . . . .	12
4.3 Workflow . . . . .	13
4.3.1 Resection planning for non-anatomical . . . . .	13
<b>5 Implementation</b>	<b>15</b>
5.1 Surface Reconstruction . . . . .	16
5.1.1 Surface contact detection . . . . .	18
5.1.2 Outlier removal . . . . .	18
5.1.3 Reconstruction Parameters . . . . .	20
5.2 Tumor Segmentation . . . . .	20
5.2.1 Initialization method . . . . .	22

5.2.2	Graph cuts . . . . .	23
5.3	Resection Planning . . . . .	24
5.3.1	Cone fitting around tumor . . . . .	25
5.4	Visualization for navigation . . . . .	26
5.4.1	Ultrasound overlay . . . . .	26
5.4.2	3D model . . . . .	27
5.5	UI Concept . . . . .	27
<b>6</b>	<b>Experiments</b>	<b>29</b>
6.1	Surface Accuracy on a technical phantom . . . . .	29
6.1.1	Methodology . . . . .	29
6.1.2	Results . . . . .	33
6.1.3	Discussion . . . . .	35
6.2	Surface reconstruction on retrospective data . . . . .	36
6.2.1	Methodology . . . . .	36
6.2.2	Results . . . . .	36
6.2.3	Discussion . . . . .	36
6.3	Usability Test . . . . .	36
6.3.1	Methodology . . . . .	37
6.3.2	Results . . . . .	37
6.3.3	Discussion . . . . .	37
<b>7</b>	<b>Discussion and Conclusions</b>	<b>39</b>
7.1	Discussion . . . . .	39
7.2	Conclusions . . . . .	39
<b>8</b>	<b>Outlook</b>	<b>41</b>
	<b>Bibliography</b>	<b>43</b>
<b>A</b>	<b>Vector and Tensor Mathematics</b>	<b>49</b>
A.1	Introduction . . . . .	49
A.2	Variable Types . . . . .	49
<b>B</b>	<b>Another Appendix</b>	<b>51</b>
B.1	Section 1 . . . . .	51
B.2	Section 2 . . . . .	51

# Chapter 1

## Introduction

### 1.1 Motivation

The goal of computer assisted surgeries is to reduce the time used to do the surgery and to also improve the surgical result for the patient. In the case of surgeries involving liver resections, navigation systems are rarely used because they do not provide enough advantages compared to the additional time needed to set them up. The accuracy of such navigation systems is affected by deformations of the liver during the surgery [13]. Additionally for registration based methods is the registration error and the time used to register the patient's anatomy to the preoperative 3D-model of the liver. Supplementary these preoperative 3D-models are very expensive and time consuming to generate. Therefore we aim to develop a new concept to navigate during liver resections. This concept should not need a preoperative scan and would therefore not need a registration. That way we would avoid the expensive and time consuming preoperative 3D-model.

### 1.2 The Liver

#### 1.2.1 Liver Anatomy

The human liver overlies the gallbladder, is located in the right upper quadrant of the abdomen and has different functions. It produces biochemicals necessary for digestion, synthesizes proteins and detoxifies various metabolites. A human liver weighs normally around 1.5 kg, is the heaviest internal organ and the largest gland of the human body. Two large blood vessels are connected to the liver: the portal vein and the hepatic artery. Both of them subdivide into small capillaries called *liver sinusoids* and then lead to the functional units of the liver known as *lobules*. To refer to the different parts of the liver, it is subdivided into eight subsegments. Each segment has its own vascular inflow and outflow.

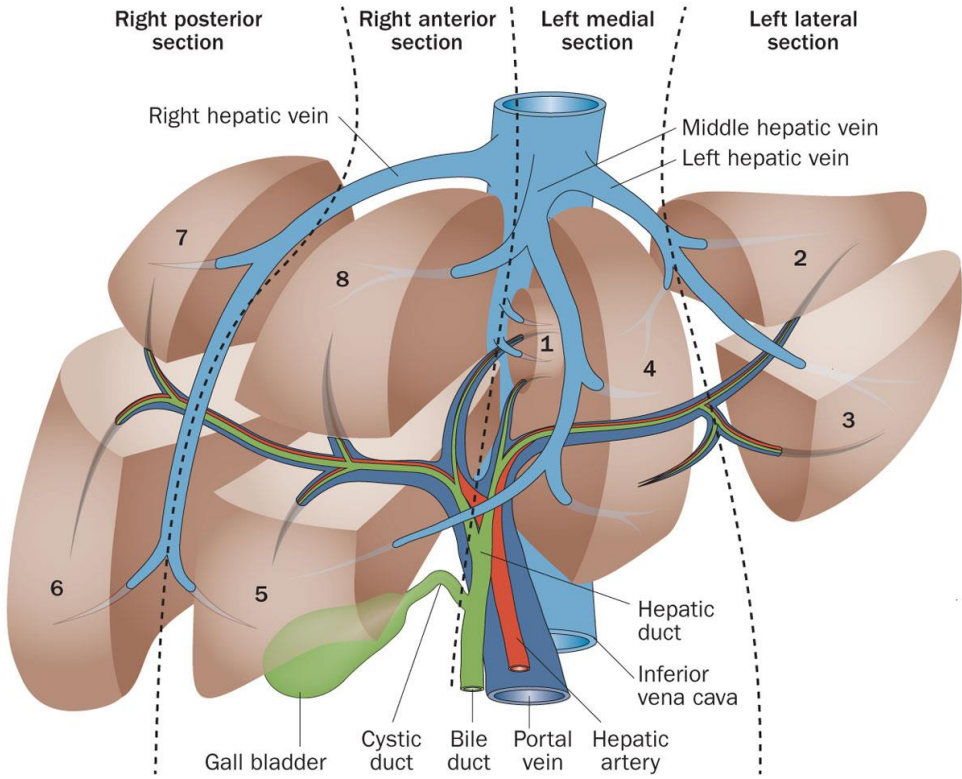


**Figure 1.1.** The liver and its eight Chouinard segments. In red is the hepatic artery which transports blood a into the liver. In dark blue the portal vein, it transports blood from the gut into the liver. All the blood leaves the liver through the hepatic veins to the vena cava [38].

### 1.2.2 Liver Cancer

Liver cancer is cancer that starts in the liver. If the cancer has spread from elsewhere to the liver, then it is known as liver metastasis. Liver metastasis are about 20 times more common than primary tumors. One of the reasons for that is the rich blood supply of the liver which helps the tumors to grow [32]. Liver cancer patients often have chronic liver diseases such as cirrhosis, problems of alcohol abuse, and viral hepatitis (B or C) [19]. The gold standard to treat liver cancer are surgical resections [26]. The liver tissue can easily regrow, given that after resection there is enough healthy tissue and blood supply preserved. Alternatively to resections one can treat liver tumors by local ablation. Both variants treat the tumors with a safety margin of 10 mm. This safety margin ensures that all tumor cells are destroyed and to prevent further spread of cancer cells [30].

### 1.3 Liver Resections

Hepatectomy is the surgical resection (removal of all or part) of the liver. Liver resections are considered major surgeries and are done under general anesthesia. Most hepatectomies are done laparoscopically. However for complicated cases also open surgeries are done [11].

Two resection techniques can be separated. Anatomical or parenchymal-sparing resections. This work will concentrate on the latter technique.

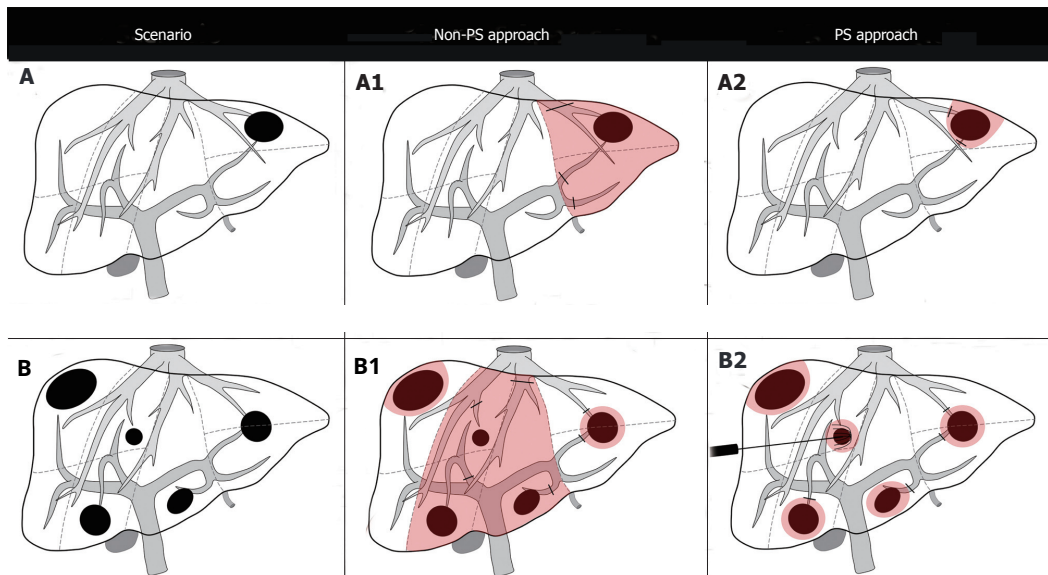


**Figure 1.2.** Two different approaches to resect liver tumors in two different situations. The *Scenario* column shows the situation of the patient's liver, the *Non-PS approach* column shows how an anatomical resection plan would look like and the *PS approach* column shows how a parenchymal-sparing resection plan would look like [6].

### 1.3.1 Parenchymal-sparing liver surgeries

[6]

## 1.4 Objectives

The objectives of this Master's thesis are:

- Implementation of the concept for an intraoperative 3D reconstruction technique of the liver from intraoperative ultrasound.
- Implementation of the intraoperative resection planning.

This work focuses on open surgical procedures of liver hepatectomies and especially parenchymal-sparing methods.



## Chapter 2

### State of the art

#### 2.1 Intraoperative ultrasound

Ultrasound imaging works by the *pulse-echo* principle. A short ultrasound-pulse is emitted from a transducer. Then the soundwaves get transmitted and reflected differently by different tissues. The reflected soundwaves travel back into the transducer and get converted into an electrical signal. After post-processing these signals become ultrasound images. Basically the ultrasound measures the mechanical properties of the tissue. The tissues have different acoustic impedance, which is the product of tissue density and ultrasound speed in travelling through the tissue. The resolution of the ultrasound images depends on the frequency of the ultrasound waves. High frequencies lead to high resolutions but low depth into the tissue because the absorption of the sound energy increases with frequency too. Therefore the useability to see deep structures is limited [40]. In liver surgeries the ultrasound is used for intraoperative planning and navigation inside the liver. Figure 2.1 shows an example of an ultrasound image of the liver and its corresponding position in the 3D liver model. The surgeon can find the tumors inside the liver by using the ultrasound. Registration methods based on 3D ultrasound reconstructed liver vessels also exist but are not used in practice a lot yet [24]. Therefore ultrasound is an important and established instrument in liver surgeries.

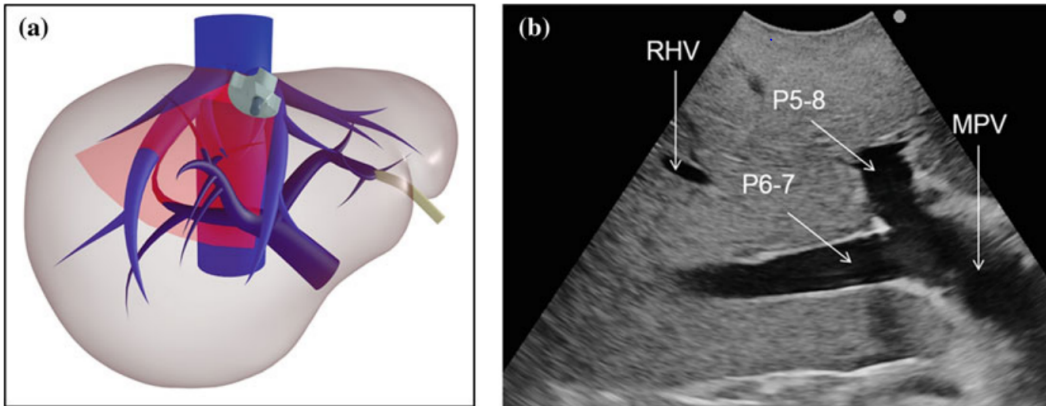


**Figure 2.1.** Left (a) ultrasound image plane in the liver. Right (b) intraoperative ultrasound image. One can see the right hepatic vein (RHV), the portal branch to segments 5 and 8 (P5-8) and the portal branch to segments 6 and 7 (P6-7) [40]

## 2.2 Navigation for liver resections

The actual intervention in computer assisted surgeries (CAS) is defined as surgical navigation. For navigated surgeries special instruments are used. These instruments are tracked by the naviagation system. The orientation and position of the instruments in relation to the patient's anatomy is visualized on a monitor in the operating room. The surgeon can then see what he does on the monitor and uses the system to navigate the location and position of its instruments. This is specially then useful when the tip of the instrument is not actually visible for the suergeon. In liver surgeries, the navigation is mostly done by first registering the patient to a pre-operative 3D computer tomography (CT) scan of the liver during the surgery. All surgical instruments have trackable markers attached to them and a tracking camera sees these markers and can differentiate the different instruments from their attached markers. The achieved navigation accuracy with such a system was  $4.5 \text{ mm} \pm 3.6 \text{ mm}$  averaged over nine surgeries [36]. Current research tries to compensate for deformations of the liver after the CT scan to the actual shape of the liver [13] [14].

### 2.2.1 Creation of preoperative 3D-models

[33] time consuming and method to create 3d-model from CT

### 2.2.2 Registration methods

Different registration methods exist. Discrete landmarks, surface scans and volumetric sonography scans are just a few of the approaches that can be used to achieve precise alignment of the preoperative image data with the surgical site [9].

### 2.2.3 Tracking modalities

To track surgical instruments and patient's anatomy (define the position and orientation in real time) during naviagated surgery a tracking system is needed. Tracking can be done by different technologies. The most used tracking modality is optical tracking.

### Optical tracking

Optical tracking is the most used tracking modality in naviagated liver surgeries. Passive markers (spherical, retro-reflective that reflect infrared light) or active markers (infrared-emitting markers that are activated by an electrical signal) [42] are attached to the objects that need to be tracked. A tracking camera is then emitting infrared light by illuminators on the position sensor (only for passive markers). The position sensor determines the position and orientation of the tracked instruments based on the information it receives from those markers [1].

## 2.3 Surface reconstruction of unorganized points

A surface reconstruction's goal is to create a surface from sampling points. Two main steps need to be processed. First, collecting the sample points. Second, apply a reconstruction algorithm to the sampled points.

### 2.3.1 Data acquisition

There exist different methods of collecting surface points [18][27][16][12][17]. Optical (non-contact scan) scans are the most popular ones. Specialy laser based scanners can scan very fast and with a precision in the order of micrometers. Also contact scans exist [34]. Contact scans can also be very precise (in the order of micrometers). Only a few articles were published in the field of liver surface scanning [31] [39]. They used stereo laparoscopic cameras to sample the surface. The resulting sampling points lie on or near an unknown surface. A reconstruction algorithm has now to reconstruct the surface from these points.

### 2.3.2 Reconstruction algorithms

Again, a lot of reconstruction algorithms exist [29], but not all of them are made to reconstruct from unorganized points. This means that the point orders, orientations, connections and the topological type of the surface is not known a priori. Therefore it is necessary that the algorithm does not assume any structure on the data points [21] [43]. The orientations, connections and the topological type must be inferred from the points. This is a major difficulty of the general surface reconstruction problem [20]. In the past few decades, many algorithms that can solve this problem have been published. Nevertheless it is still a chal-langing task that is part of current research [28]. The available reconstrction types can be classified into two groups: implicit volume-based and explicit mesh-based reconstructions.

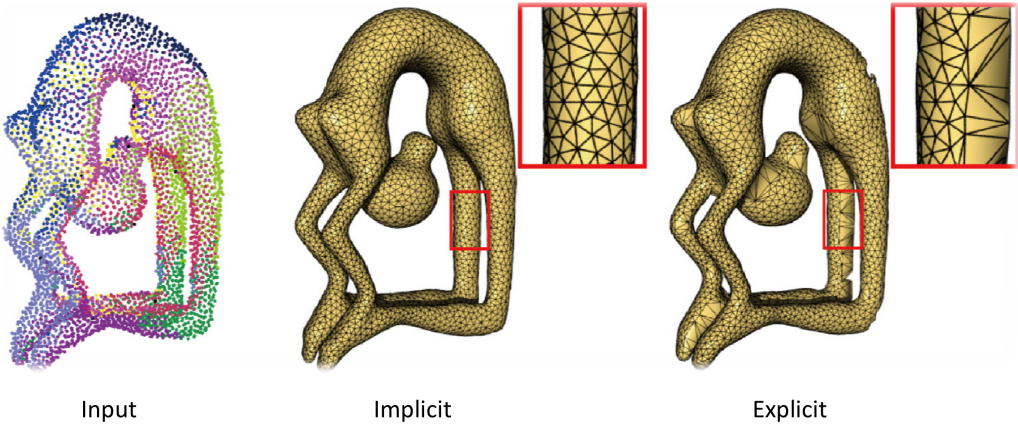


**Figure 2.2.** The difference between implicit and explicit surface reconstructions. On the left side is the pointcloud used as input. In the middle the result of an implicit reconstruction. On the right side the result of an explicit reconstruction [2]

#### Explicit mesh-based reconstruction

Explicit mesh-based reconstruction methods form a triangular mesh directly from the unorganized points. These mesh-based reconstructions are precise but they have problems with noise, complex shapes and especially holes in data.

#### Implicit volume-based reconstruction

Implicit volume-based reconstruction techniques construct an implicit volume-function from the input points. From the iso-surface of the volume-function a restored surface can then be obtained. For these methods it is not a problem if the surface topology is complex. But most of these methods suffer from oversmoothing the data and the need of accurate directions of normal vectors in addition to the unorganized points.

[22] oriented point set hornung2006robust [21] non uniformly sampled point clouds without normal information [43] NN to reconstruct from unorganized points

## Chapter 3

### Problem Statement

To make computer assisted navigation in liver resection surgeries more accessible to liver surgeons, a new concept has to be developed in order to do some first testings. Specifically, the method should fulfill the following:

- The software should guide the surgeon through the surgical procedure.
- A 3D-model of the liver should be created during the surgery.
- The planning for the resection of the tumor should be done intraoperatively on the created 3D-model.
- The method should be ready for testings in the OR.



## Chapter 4

# Concept

In this chapter the desired concept will be presented.

### 4.1 System

The hardware used with this system consists of:

- a tracked ultrasound device
- a tracked pointer tool
- an optical tracking camera to track the instruments
- a computer to run the software
- a 3D-monitor which displays the 3D contents of the software
- a touch-screen on a 2D-monitor to operate the software and show the ultrasound images

The software in this system consists of:

- a sampling method to collect points on the liver-surface
- a reconstruction method to reconstruct the surface from the sampled points
- a segmentation method to segment the tumors on the ultrasound images
- a planning method to plan the resection of the liver
- a navigation mode used to navigate during the removal of the tumor

### 4.2 Functionalities

The three main functionalities of the developed concept will be presented in this chapter. These functionalities were specifically developed for this project.

### 4.2.1 Surface Reconstruction

During surgery ultrasound images and their corresponding 6D poses (positions and orientations) are collected and analyzed. First each ultrasound image has to be checked for contact with the liver. If the ultrasound passes the check, that means the ultrasound image looks like an ultrasound image that can only arise when the ultrasound probe lies on the liver surface, then the position of this image can be used.

In order to use the sampled position corresponding to an image, this position has to be transformed into the correct coordinate system first. There are four different coordinate systems. The first coordinate system is the image coordinate system. The units in the image coordinate system are pixels and the origin is in the top left corner of the image. The second coordinate system is the ultrasound coordinate system. The origin of this coordinate system is at the probe tip in the middle and the units in this and the following coordinate systems are millimeters. The third coordinate system is the ultrasound-tool-marker coordinate system. The origin is at a user defined location, relative to the reflective marker spheres. The final coordinate system is the tracking camera coordinate system. The origin of this coordinate system is at the position sensor in the tracking camera and can not be changed.

At the end of this transformation chain, a image pixel 2D position was transformed into a tracking camera 3D positon and the units changed from pixel to millimeter. This 3D location in the tracking camera coordinate system will be added to the collection of points to later reconstruct the surface from.

After collecting the surface points, the reconstruction algorithm from Hoppe [20] reconstructs the surface from these points.

### 4.2.2 Tumor Segmentation

To reconstruct and later plan the resection of a tumor, the shape of the tumor has to be made visible first. Because most liver tumors are not visible from the outside of the liver, an ultrasound device is often used during liver resections to look behind the liver surface.

Therefore this ultrasound device should also be used to reconstruct the shape of a tumor. This is done by segmenting the same tumor on multiple ultrasound images. Depending on the desired resolution of the reconstructed tumor, more or less images have to be segmented. With the corresponding poses of the ultrasound images, the 3D positions of the individual contour pixels can be calculated. These positions will create a point cloud that represents the shape of the tumor. This shape can then be reconstructed by a surface reconstruction algorithm.

#### Semi automatic 3D

In order to semi automatically segment a tumor in the liver, the segmentation has to be initialized manually. To do so, a sphere needs to be placed in the center of the tumor manually. Afterwards each ultrasound image which cuts this sphere will be segmented automatically with the cutted area as an initialization for the segmentation. These segmentations would be used to reconstruct the surface of the tumor.

### 4.2.3 Resection Planning

For parenchymal-sparing liver resections, the goal is to keep as much healthy tissue as possible. When the tumor's location in the liver and the size are known, one can plan a precise resection from these informations. The surgeon is able to choose which shape the

resection plane will have and how much safety margin he wants to add around the tumor. Then a resection plane which fulfills the desired requirements will be shown to the surgeon. This resection plane could then be fine tuned before the surgeon starts the resection.

### 4.3 Workflow

In this section the conceptual workflow through a liver resection using the desired system will be presented. The following flow diagram shows the five main steps (Figure 4.1).

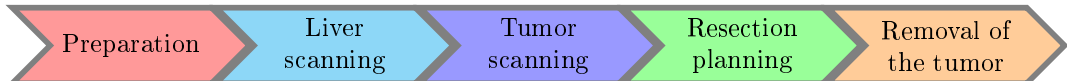


**Figure 4.1.** The main steps the surgeon has to do during a surgery with the proposed system.

In the preparation step the patient is prepared for the surgery, the navigation system is setup in the operating room and the software is started. Then the tools are setup. Afterwards the surgery starts, the intervention starts and the liver gets prepared for the resection. Subsequently step two starts. In this step the surgeon scans the liver surface with an ultrasound probe. He does that till a 3D model of the for the surgery needed part of liver is reconstructed. Thereafter follows the tumor scanning step. Here the surgeon locates a tumor using the ultrasound probe again. Then he freezes the ultrasound image and initializes the segmentation of it. After this the surgeon moves the ultrasound probe in different directions such that the ultrasound images cut through the tumor. He does that till the tumor is accurately enough reconstructed. Afterwards follows step four. To plan the resection the surgeon has to select the shape of the resection plane he wants to apply for this resection intervention. If necessary he adjusts the resection plane manually. Finally he uses the created model and planning to resect the tumor.

#### 4.3.1 Resection planning for non-anatomical ...



## Chapter 5

### Implementation

This chapter will explain how the described concept has been implemented. First an overview of the concept and then the main parts of the software in more detail. The trackable marker is attached to the ultrasound probe. The marker is detectable by the tracking camera and enables the camera to determine the position and orientation of the ultrasound probe. The probe on its own will create an ultrasound image. Then the sampled ultrasound image and pose will be post processed as a pair in the computer. In the software, depending on the actual state of the surgery, the use of the two will be different.

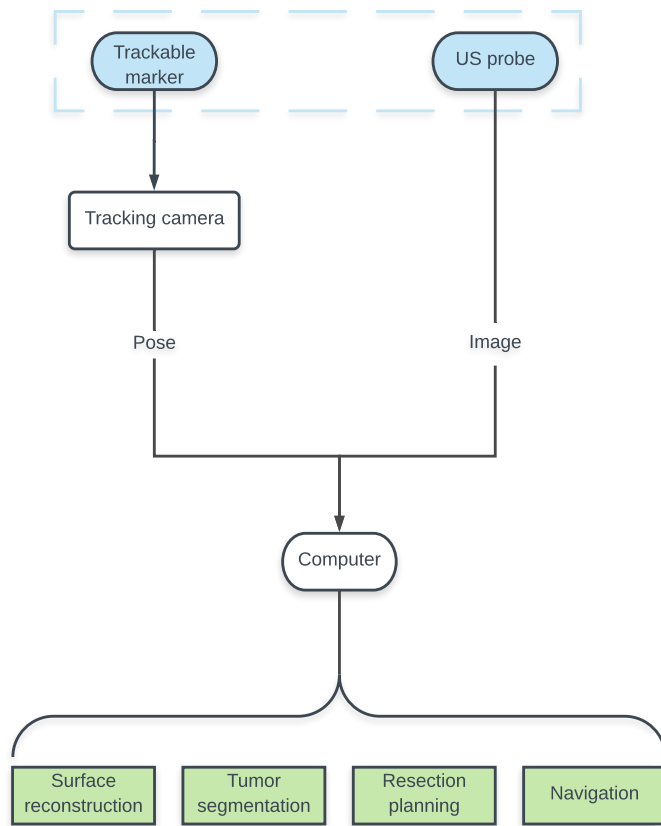


**Figure 5.1.** The way of the ultrasound image and the corresponding pose to the computer and later to the different parts in the software.

## 5.1 Surface Reconstruction

While the surgeon is scanning the surface, the software in the background filters out unusable positions. An image pose pair has to take two hurdles to become accepted in the group of surface points. The image has to prove that it arised from the liver surface and the position has to have a similar distance to its neighbors as its neighbors to it. When enough points are sampled, the reconstruction of the surface will be carried out.

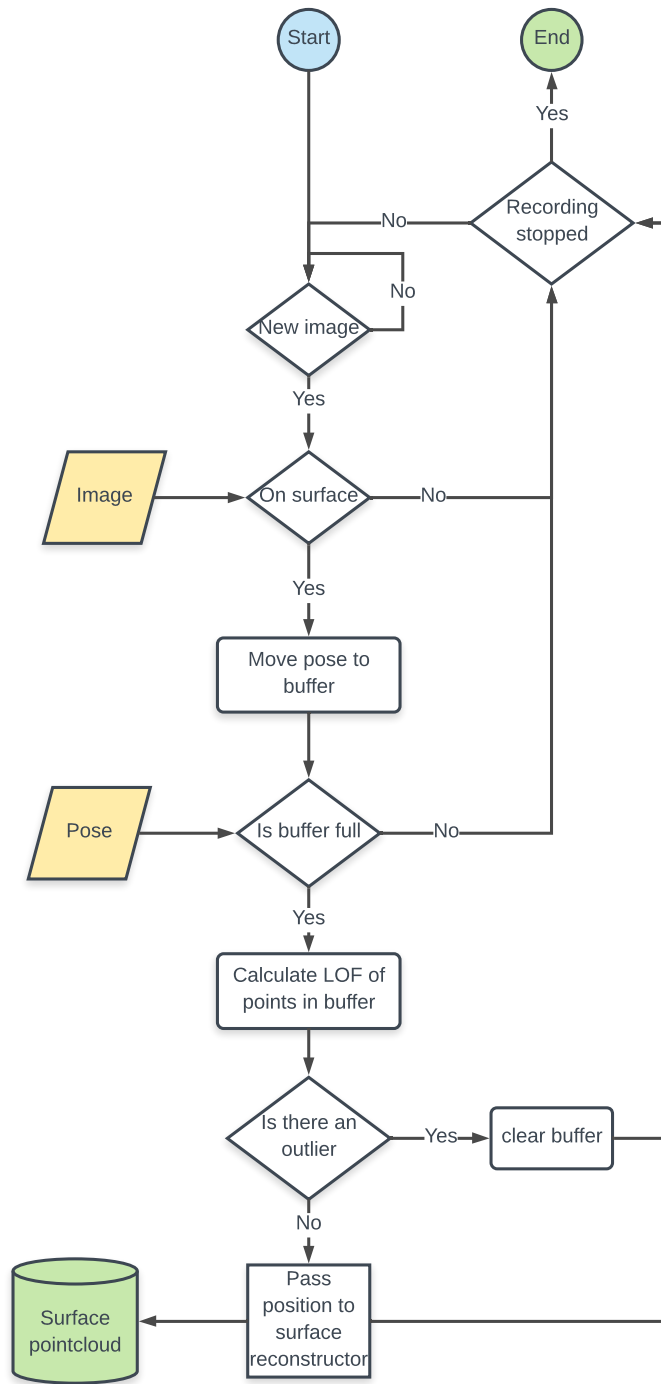


**Figure 5.2.** The way of the image and its pose if the surgeon is scanning the surface.

### 5.1.1 Surface contact detection

For an image pose pair, the first step to pass is the contact detection. Only the ultrasound image is needed in this step.



**Figure 5.3.** Three ultrasound images from left to right: No contact with the liver, difficult to decide (In this case it would be contact because the middle part of the image shows contact), contact with the liver

A classifier detects whether the US probe has contact to the liver or not. Therefore, a support vector machine (SVM) was trained with US images from the phantom and from previous navigated liver surgeries. The SVM was trained to classify the image into “no surface contact” (left) and “surface contact” (middle and right). The images were labelled as “surface contact” if at least 50% and the center had contact to the surface (Figure 6.4 middle). The classifier takes into account that US waves are reflected at the US probe-air interface when the US probe has no contact to the liver and therefore no image is formed. The features for the classifier were: mean, median, minimum, maximum, variance, skewness and kurtosis of the pixel values. All features are calculated on the upper half of the image. For training, a set of 2'311 images (1'056 with contact, 1'255 without contact) were used. The training data was composed of images from a phantom (88%) and images from previous navigated liver surgeries (12%). All computations were performed using the SciPy software package. When the image is classified as “surface contact”, then the position of the pose is stored into the buffer. The buffer has a capacity of 10 positions. When the addition of the actual pose leads to a full buffer, the buffer is tested for outliers. Each time a “no surface contact” image is classified and the positions buffer is not empty it gets cleared.

### 5.1.2 Outlier removal

To find outliers in the current buffer the local outlier factor is calculated for each position.

#### Local outlier factor

The local outlier factor is a numerical value that describes the local density of a position compared to its k-nearest neighbors (Figure 5.4).

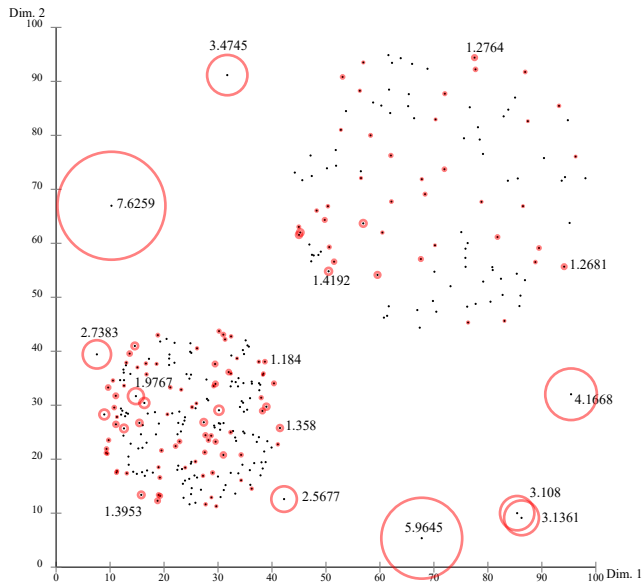


**Figure 5.4.** Example of the local outlier factors in a two dimensional pointcloud [15].

Five steps can be separated to find the LOF of one position.

1. For each point calculate the distance to all the other points in the buffer
2. For each point find the distance to his k-nearest neighbor → *k-distance*
3. Find the *reachability distance* from the k-nearest neighbors of each point to it self
4. Calculate the *local reachability density* for all points
5. Calculate the *local outlier factor*

The *reachability distance* of point *A* from another point *B* is defined:

$$\text{reachability-d}_k(A, B) = \max\{\text{k\_d}(B), d(A, B)\}$$

The *k-distance* of point *B* depends on its k-nearest neighbors and does not need to include point *A*. But the actual distance between point *A* and *B* depends on only *A* and *B*. The larger of the two will be the *reachability distance* of point *A* from point *B*.

The *local reachability density* of a point *A* describes its neighborhood and is defined by:

$$\text{LRD}(A) := 1 / \left( \frac{\sum_{B \in kNN(A)} \text{reachability-d}_k(A, B)}{|kNN(A)|} \right)$$

In words this is the inverse of the sum of the *reachability distances* of point *A* from its k-nearest neighbors devided by *k*.

Finally the *local outlier factor* of a point *A* indicates how his neighborhood compares with the neighborhoods of his k-nearest neighbors. The LOF of *A* is defined by:

$$\text{LOF}(A) := \frac{\sum_{B \in kNN(A)} \text{LRD}(B)}{|kNN(A)|}$$

If the neighborhood of  $A$  is very similar to the neighborhoods of its  $k$ -nearest neighbors, the LOF is close to 1. If its neighborhood is less dense than the neighborhoods of his  $k$ -nearest neighbors, the LOF becomes larger than 1. If its neighborhood is more dense than the neighborhoods of his  $k$ -nearest neighbors, the LOF becomes lower than 1.

If an outlier is found in the buffer, the whole buffer is cleared. In the case that no outlier is found, the oldest pose in the buffer gets moved into the point collection to reconstruct the surface from.

### 5.1.3 Reconstruction Parameters

Finally there is a pointcloud with all the collected positions. This pointcloud will be used as input for the surface reconstruction algorithm by Hoppe [20]. The algorithm consists of three phases. From an unorganized set of points, phase 1 constructs an initial dense mesh. Starting with the dense mesh created in phase 1, phase 2 reduces the number of faces and improves the fit to the data points. In phase 3, the surface representation is changed from a piecewise linear one (meshes) to a piecewise smooth one. For the computations the implementation in VTK (SurfaceReconstructionFilter) was used. The two main parameters of this reconstruction algorithm have been optimized by applying the grid search method.

#### Grid search for parameter optimization

The *neighborhood size* and the *sample spacing* are the variable parameters of the used surface reconstruction algorithm. The *neighborhood size* specifies the number of neighbors each point has. These neighbors are used to estimate the local surface orientation. The *sample spacing* sets the spacing of a 3D sampling grid. To find the optimal values to use in the algorithm with the point cloud data produced in the experiment described in section 6.1, a first, rough grid search has been done to find the range of interest of the two parameters. The same data was then used to do a second, more dense grid search over the range of interest (Figure 5.5 and 5.6). For each parameter setting, the average distance from the reference points to the reconstructed surface was calculated. The found mean distance varies from 5.1 mm to 3.9 mm. Neighborhood sizes smaller than 8 show an increase of the mean distance for sample spacings larger than 25 mm. Neighborhood sizes over 30 seem to increase the mean distance also. The standard deviation of the mean varies between 6.1 mm and 4.6 mm. These high deviations result mostly from the boarder part of the reconstructions where the reference points are more than 2 cm away from the surfaces (see section 6.1). One can say the standard deviation of the mean decreases together with the neighborhood size used for the reconstruction. But this is only true for neighborhood sizes larger than 13. Because from neighborhood size 13 till 10 the standard deviation increases not till then it decreases again. By simply summing up the mean and the standard deviation, one finds that the optimal parameters for the tested surface samplings are 13 for the neighborhood size and 30 mm for the sample spacing.

## 5.2 Tumor Segmentation

The flow diagram in figure 5.7 helps to understand the following explanation of the creation of a tumor 3D model. To create a 3D model of a tumor, the surgeon has to freeze an ultrasound image such that the real tumor center is visible on this image. To find the location of the tumor's center, the surgeon locates the tumor with the ultrasound. Then he

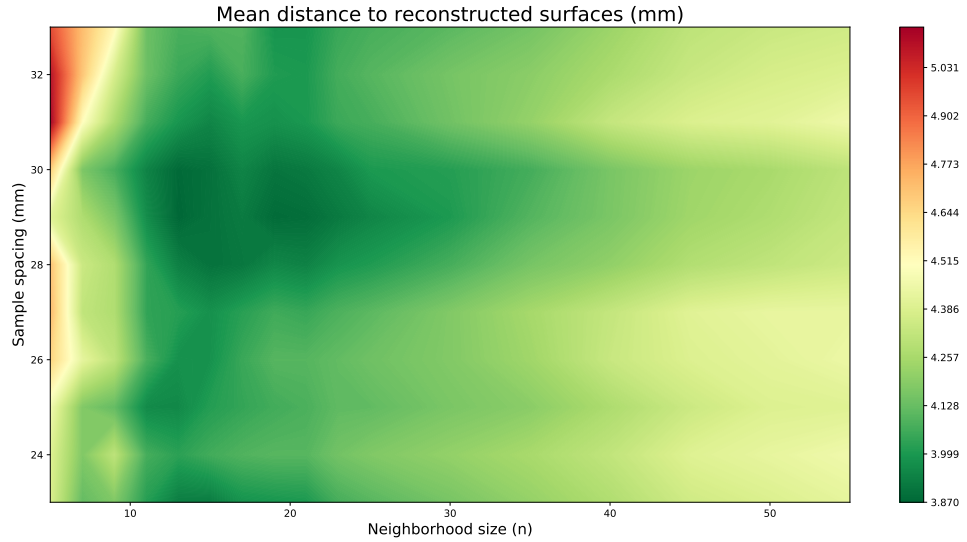


**Figure 5.5.** This contour plot shows the mean distance calculated over 10 differently sampled point collections. All point collections represent the surface of the same liver phantom.

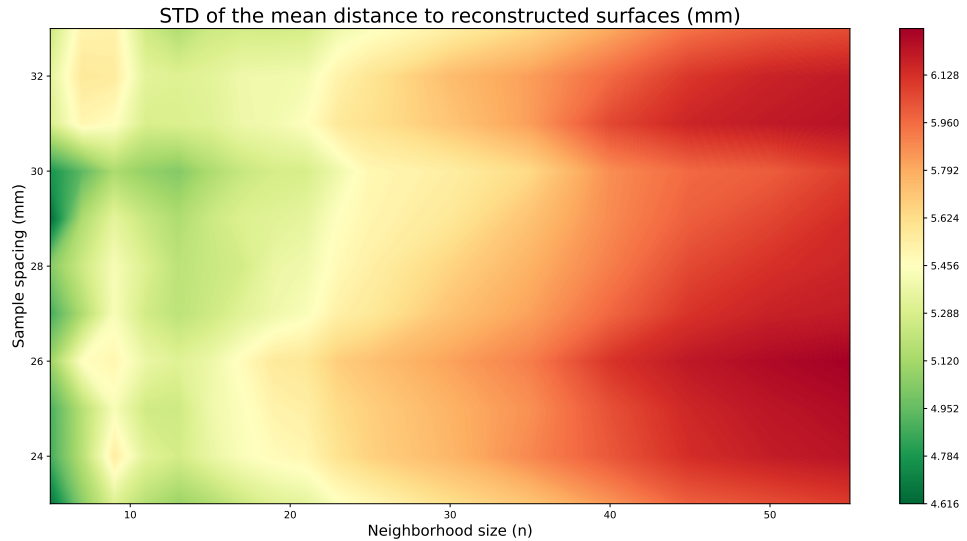


**Figure 5.6.** This contour plot shows the STD of the mean distance calculated over 10 differently sampled point collections. All point collections represent the surface of the same liver phantom.

freezes the ultrasound image that cuts through the middle of the tumor. The 6D pose of that ultrasound image is stored and the image is passed to the next step.

Most tumors have roundish shapes, and a sphere is the easiest geometrical shape that can be used to approximate a tumor's real shape. To define a sphere two components are needed: the location and the radius of the sphere.

To get more information about the tumor, the tumor on the freezed image has to be segmented. This segmentation is done semi automatically. That means the surgeon has to

roughly initialize the segmentation manually and then the graph cut algorithm implemented by openCV will segment the tumor. From the resulting segmentation shape, the tumor center and radius are estimated. The center corresponds to the mean of the segmented boarder pixels and the radius is the mean between the largest and the shortest distance from the boarder pixels to the estimated center pixel. By using the 6D pose corresponding to the ultrasoud image used for the segmentation, the center pixel gets transformed into the tracking camera coordinate system. Finally the sphere that approximates the tumor can be drawn into the same coordinate system as the liver surface.

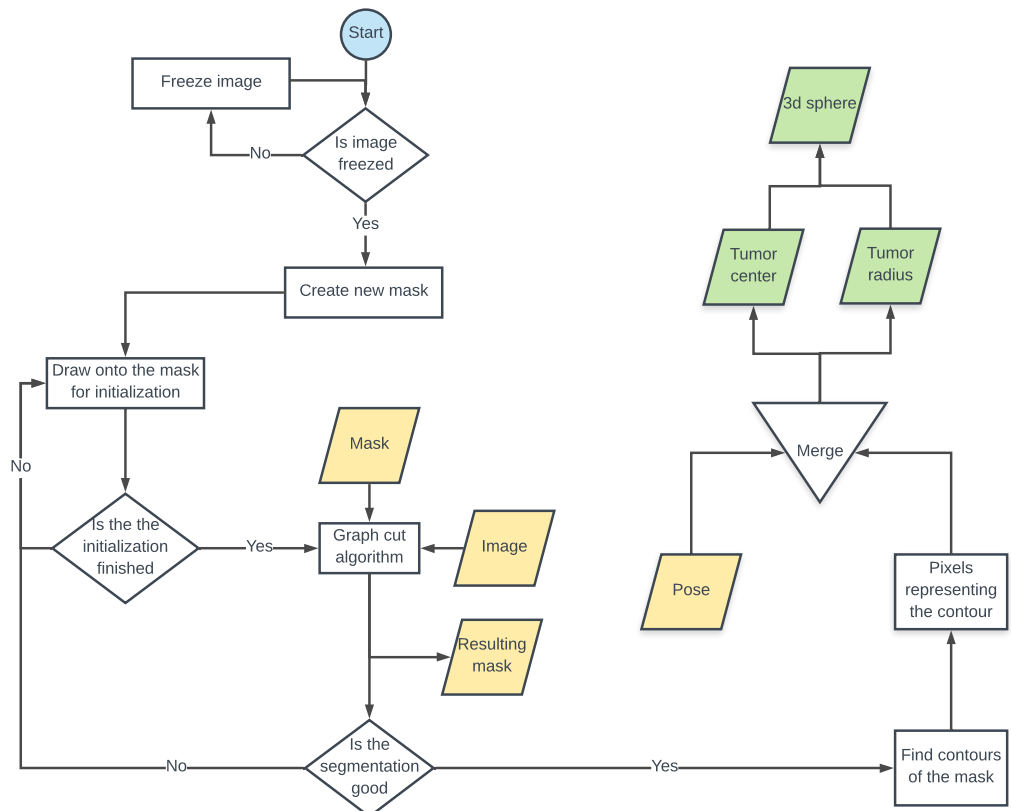


**Figure 5.7.** The way of the image and its pose if the surgeon is scanning the surface.

### 5.2.1 Initialization method

As explained in section 5.2, the segmentation of the tumor has to be initialized manually. This is done by drawing onto an initialization mask. The surgeon draws two circles onto the mask. After clicking in the middle of the tumor, two circles are drawn onto the mask. An orange circle for the pixels that should be looked at to find the boundary of the tumor (Figure 5.8). And a red circle to color pixels surely originating from the tumor. Most of the time the two circles need to be increased or decreased in size. This is done by clicking the plus or minus buttons. Both circles are changed at the same time. The position can be changed by using the arrow buttons. As soon as the surgeon is satisfied, he confirms the

initialization and the created initialization mask is passed to the segmentation algorithm.

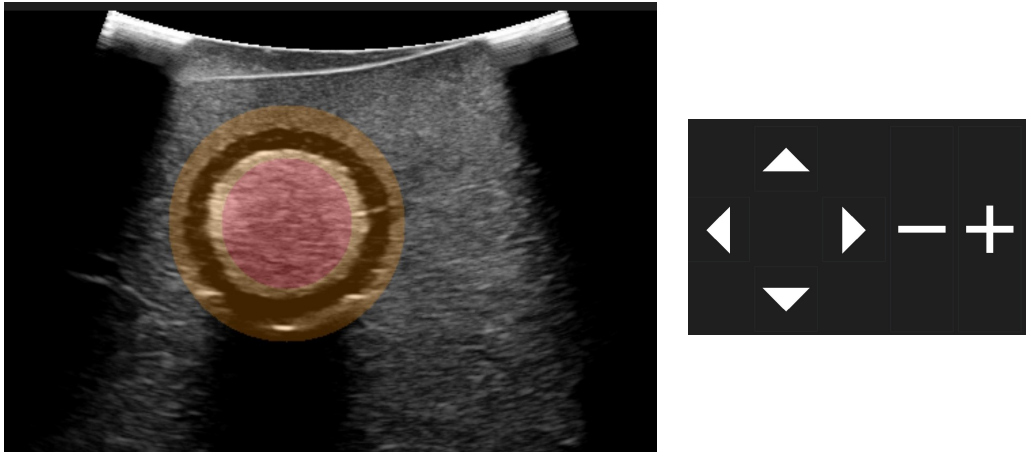


**Figure 5.8.** On the left side: Initialization drawing for the segmentation of the tumor. Red the pixels which are tumor pixels. And orange the pixels that are from the tumor or the background. The not colored pixels represent background. On the right side: Controls to manipulate the initial segmentation.

### 5.2.2 Graph cuts

For the segmentation a graph cuts algorithm is used. This algorithm treats pixels as set of nodes connected in a graph (Figure 5.9). Foreground and background are initialized by selecting parts in the image. Pixels labeled foreground belong to the source and background labeled ones to the sink. The nodes (pixels) are connected to their neighbors, the source, and the sink by edges whose weights are defined as follows:

- Node to source → Probability of the node to belong to the source (foreground)
- Node to sink → Probability of the node to belong to the sink (background)
- Node to adjacent node → Similarity measure to its neighboring node.

A weight of an edge to adjacent node depends on the similarity between pixel intensities. The edges between adjacent nodes, initialized to the same label, have an infinitely high weight [41].

After calculating all the weights in the graph, it has to be cutted in order to create a segmentation. All pixels not assigned already in advance foreground or background will get assigned by cutting the graph. The segmentation is obtained in form of a min-cut [8] in which edges are removed to separate source and sink, and sum of their weights is minimized. This way you can find a group of foreground and background pixels.

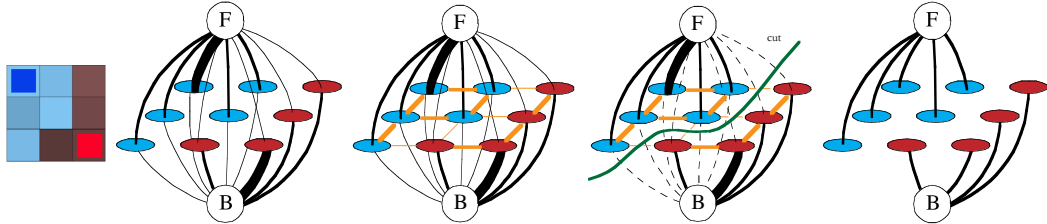


**Figure 5.9.** From left to right the steps of a graph cut segmentation. The first image shows the nine pixels to separate into foreground and background. A clear blue and a clear red drawing onto two pixels indicate the initialized foreground and background. The second image illustrates the probabilities of each pixel belonging to the foreground or the background. The third image shows the edges between neighboring pixels in orange. Finally the last image shows the edges to be cut as dashed lines. Finally the last image shows the result for foreground and background [8].

### 5.3 Resection Planning

The 3D models of the liver and the tumor are created. In this section we will explain how the resection plane is calculated and displayed in the 3D scene. In order to make better planning possible, the nearest point to the tumor center on the surface of the liver must first be determined. To find this point, the *vtkCellLocator* class is used. This class has a function that can be used to find the nearest point on a surface to a given point and the distance between them. The found point and distance together with the polygonal data of the liver surface, tumor, value for the safety margin, and the desired resection shape are then passed into the resection calculator (Figure 5.10).

The resection calculators task is to create a resection plane under the given conditions and to represent it in the 3D model. It also shows the safety margin taken into account as a sphere around the tumor. In addition, also a help line is displayed on the liver surface to show where the surgeon could start the resection.

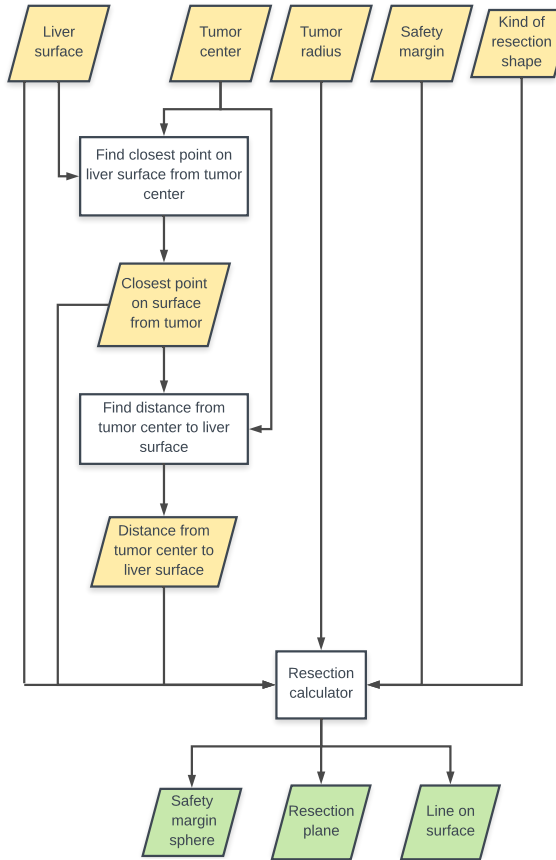


**Figure 5.10.** This flow chart shows the data flow to and from the resection calculator.

### 5.3.1 Cone fitting around tumor

In order to keep as much healthy tissue as possible and still remove the tumor while maintaining the necessary safety margin around the tumor, the resection plane is recalculated for each tumor. Depending on the distance ( $d$ ) between tumor center ( $C$ ) and liver surface the angle  $\alpha$  varies between  $10^\circ$  and  $30^\circ$ . For tumors with a distance less than 10 mm the angle is fixed to  $30^\circ$  and for distances larger than 30 mm the angle is fixed to  $10^\circ$ . The direction of the cone is defined by the vector from the tumor center to the nearest point ( $P$ ) on the surface. After constraining the cone to be tangential to the sphere of the safety margin on both sides, the position of the cone apex ( $A$ ) can be calculated. By additionally forcing the cutting of the cone tangential to the sphere of the safety margin, the length of the cone is limited towards the apex. The base of the cone is defined to be 10 mm further away from the tumor than the surface point.

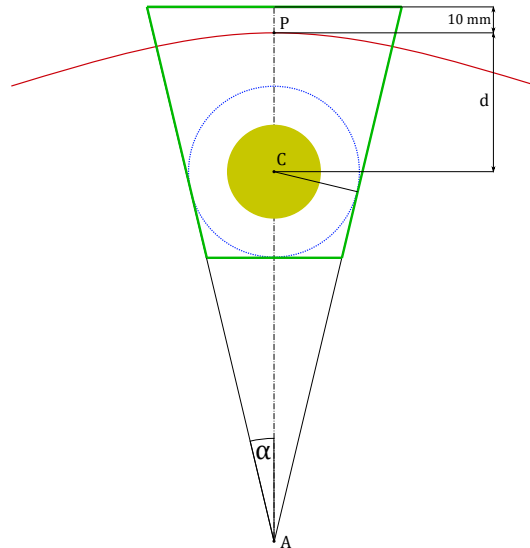


**Figure 5.11.** The geometrical shape of the resection plane (green) after fitting it around the safety margin (blue). The angle  $\alpha$  depends on the distance ( $d$ ) between the tumor center (C) and the closest point (P) on the liver surface to it. The position of the apex (A) can be calculated after constraining the safety margin to be tangential to the sides of the cone.

## 5.4 Visualization for navigation

### 5.4.1 Ultrasound overlay

The ultrasound image ...

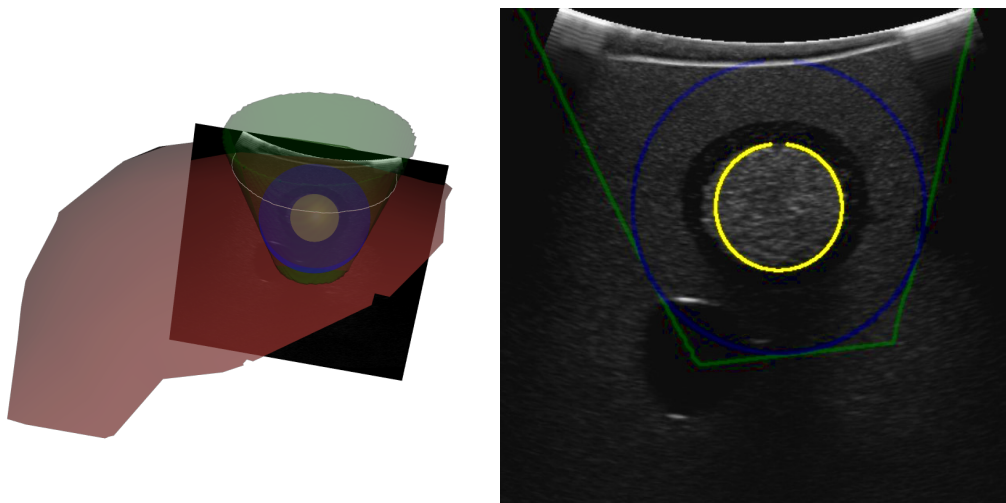


**Figure 5.12.** On the left side is the 3D scene with the ultrasound image cutting through the tumor, safety margin and the resection plane. On the right side is the resulting cutting overlay on the live ultrasound image.

5.4.2 3D model

5.5 UI Concept



## Chapter 6

# Experiments

In this chapter .... experiments will be presented.

### 6.1 Surface Accuracy on a technical phantom

The work presented in this section was presented at CURAC, Luca

Surgical resection is the gold standard for curative care for primary and secondary hepatic tumors. This procedure usually involves removing the segment of the liver where the tumor is located. In this treatment, it is important to spare enough healthy parenchyma to preserve the function of the liver after surgery. Therefore, non-anatomical resection approaches are becoming more popular, as they try to spare as much healthy tissue as possible. This way, only the tumor and a safety margin of 5 – 10 mm are removed which allows multiple resections and re-treatments in case of recurrence [4]. However, especially in these non-anatomical resections, maintaining the safety margin is challenging as the tumor is removed by cutting around the tumor in a conical or wedge shape rather than a plane along anatomical landmarks. Therefore, image-guidance systems have been introduced to guide the surgeon to precisely follow a planned resection path. These systems rely on tracking devices (optical or electromagnetic) to measure the pose of the surgical instruments and use a registration process to align a preoperative model with the patient intraoperatively [25][9]. However, the setup and use of such systems is time consuming, complex and requires extensive training, which is a major reason why they are not widely used [23]. Additionally, the registration process introduces errors due to organ deformation between the image acquisition and the surgery. During conventional, non-anatomical resections a resection plan is drawn onto the liver before the start of the resection. Therefore, an important part of the resection plan is an accurate reconstruction of the liver surface. This surface is then used to project the outline of the tumor and a safety margin onto the surface. This is where the surgeon would start with the transection of the parenchyma. Previous work used such surface reconstructions based on laser scanners [37] for intraoperative registration, which requires additional equipment. In this study, we evaluated an ultrasound (US) based method to automatically reconstruct the liver surface intraoperatively.

#### 6.1.1 Methodology

The image processing pipeline consists of three steps, the acquisition, the contact detection and the surface reconstruction (Figure 6.1). First the data from an ultrasound scanner (Flex focus 800, BK Medical, Denmark) and a tracking camera (Polaris, NDI, Canada) is

acquired and fused on a navigation system (CAS-One Vario, CAScination AG, Switzerland) for liver surgery. Then each image is classified whether it has contact to the liver surface or not. The position of the images with contact to the liver surface are then further processed in the surface reconstruction step to create a model of the liver surface. The result is then visualized in a 3D viewer.

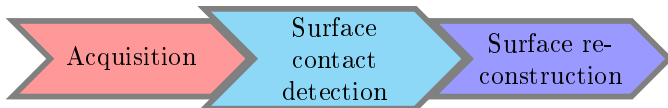


**Figure 6.1.** The data processing pipeline

### Acquisition

During the data acquisition phase, the ultrasound image and the corresponding 6D pose are recorded using the navigation system. The ultrasound was calibrated using a Z-wire phantom [35] and is tracked by an optical tracking system. To simulate a liver surgery, a multimodal liver phantom (Figure 6.2) and an intraoperative ultrasound was used to get the ultrasound images. During the simulation the ultrasound device had a trackable and calibrated marker attached. To find an optimal sampling method, the liver was scanned with six different techniques (Figure 6.3). The two spiral techniques represent recordings of moving the US device to draw a spiral onto the liver. Either from the center to the peripheral part (spiral out) or vice versa (spiral in). The two sweep techniques represent recordings of moving the US device left and right (Sweep LR) or forward and backward (Sweep FB). The flower technique represents a recording of moving the US-device to draw a flower onto the liver. Additionally, a point grid was acquired as reference points for evaluation of the other reconstructions.



**Figure 6.2.** The US liver phantom used for the experiments in this study

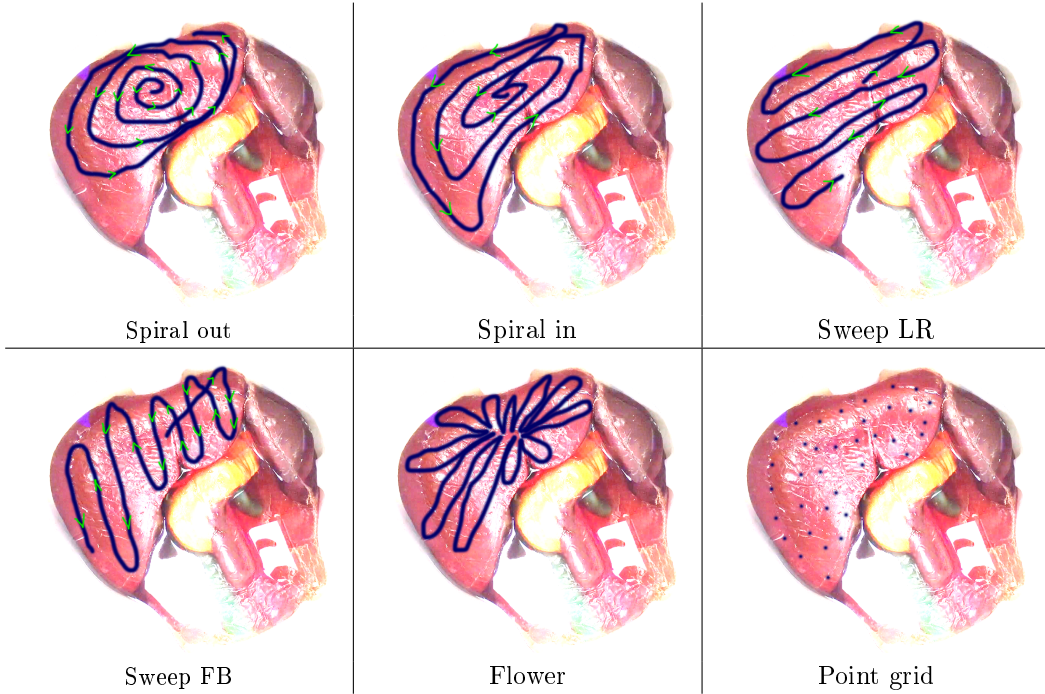


**Figure 6.3.** Different sampling movements of the ultrasound device over the surface of the liver

#### Surface contact detection

In the surface contact detection step, a classifier detects whether the US probe has contact to the liver or not. Therefore, a support vector machine (SVM) was trained with US images from the phantom and from previous navigated liver surgeries. The SVM was trained to classify the image into “no surface contact” (left) and “surface contact” (middle and right). The images were labelled as “surface contact” if at least 50% and the center had contact to the surface (Figure 5.3 middle). The classifier takes into account that US waves are reflected at the US probe-air interface when the US probe has no contact to the liver and therefore no image is formed. The features for the classifier were: mean, median, minimum, maximum, variance, skewness and kurtosis of the pixel values. All features are calculated on the upper half of the image. For training, a set of 2'311 images (1'056 with contact, 1'255 without contact) were used. The training data was composed of images from a phantom (88%) and images from previous navigated liver surgeries (12%). All computations were performed using the SciPy software package.

#### Surface reconstruction

To reconstruct the surface of the liver from the sampled points, the surface reconstruction algorithm by Hoppe et al. [20] was used. The algorithm consists of three phases. From an unorganized set of points, phase 1 constructs an initial dense mesh. Starting with the dense mesh created in phase 1, phase 2 reduces the number of faces and improves the fit to the data points. In phase 3, the surface representation is changed from a piecewise linear one (meshes) to a piecewise smooth one. For the computations the implementation in VTK (SurfaceReconstructionFilter) was used (neighborhood size of 50 and sample spacing of 10).

Due to the different latencies of the US and the tracking system (with the US being slower), a delay of 4 frames (0.2 seconds) is applied to the tracking data.

### Experimental evaluation

For evaluation of the surface detector the data was split into training (80%) and test data (20%). The precision and recall were calculated for performance analysis on the test set. To quantitatively evaluate the reconstructed surfaces, the points of the point grid measurement (414 points) were used as a reference. These reference points represent points on the surface of the liver in an undeformed state. For each of these reference points, the error is computed as the shortest distance to the reconstructed surface. All computations were performed using SciPy.

### 6.1.2 Results

Overall, the surface contact detector was evaluated on a test set with 2414 images. Additionally, 10 scans of the liver surface were evaluated against the reference points to measure the accuracy of the surface reconstruction.

### Surface contact detection

To evaluate the contact detector, a test set of 2414 images with 50% contact and 50% no contact was used. The detector has a sensitivity of 0.95 and a specificity of 0.98. Out of all negative samples, 1.9% were detected as having contact. The prediction of one image takes 15 ms where most of the time (approx. 99%) is spent for feature extraction.

### Surface reconstruction

#### Visual assessment

The reconstruction of the liver surface created lead to a smoothed version of the measured surface part. The measured surface corresponds to the surface of the liver (Figure 6.2). However, the reconstructed surface area is larger than the sampled part of the surface. This is a property of the algorithm, as it estimates a rectangular grid.

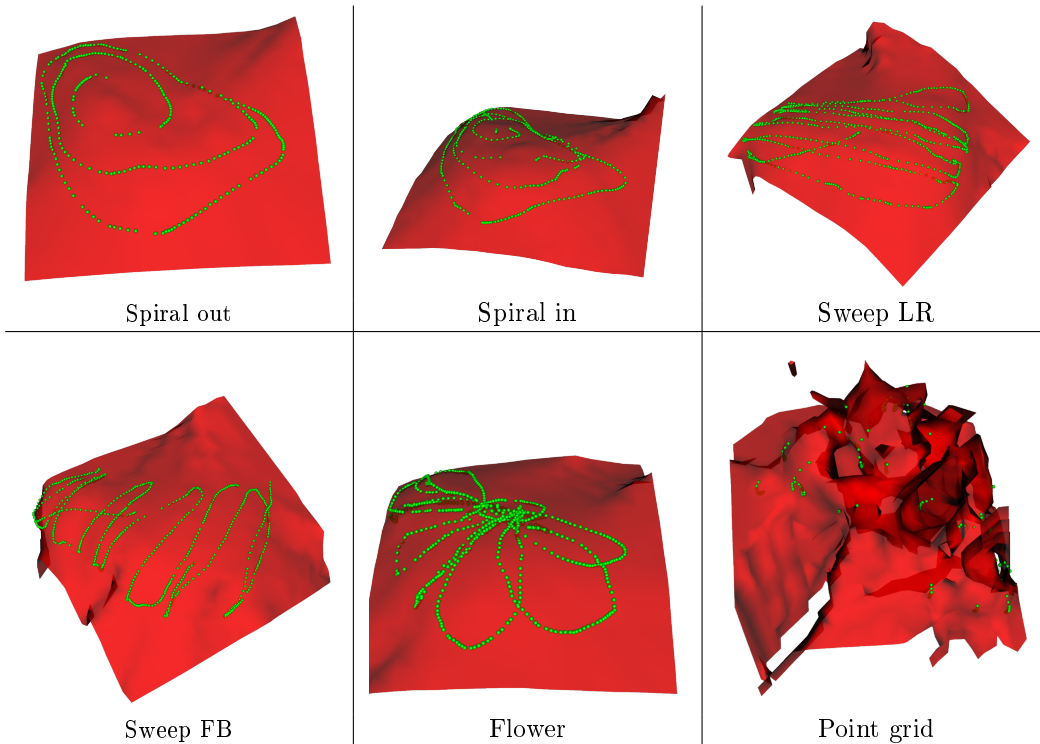


**Figure 6.4.** Reconstructed surfaces from different movements of the ultrasound device over the surface of the liver model. The names correspond to the movement drawings in figure 6.3

#### Quantitative analysis

To evaluate the accuracy of the reconstructed surfaces, the shortest distance of the reference points to the surface were computed. The overall median error for all the measurements is 2,5mm with an interquartile range of 1 mm – 5 mm. By projecting these errors corresponding to each reference point onto the liver surface, one can see that the highest errors are in segments 2 and 3 And the lowest in segments 4, 5, 6 and 8 (Figure 6.5).

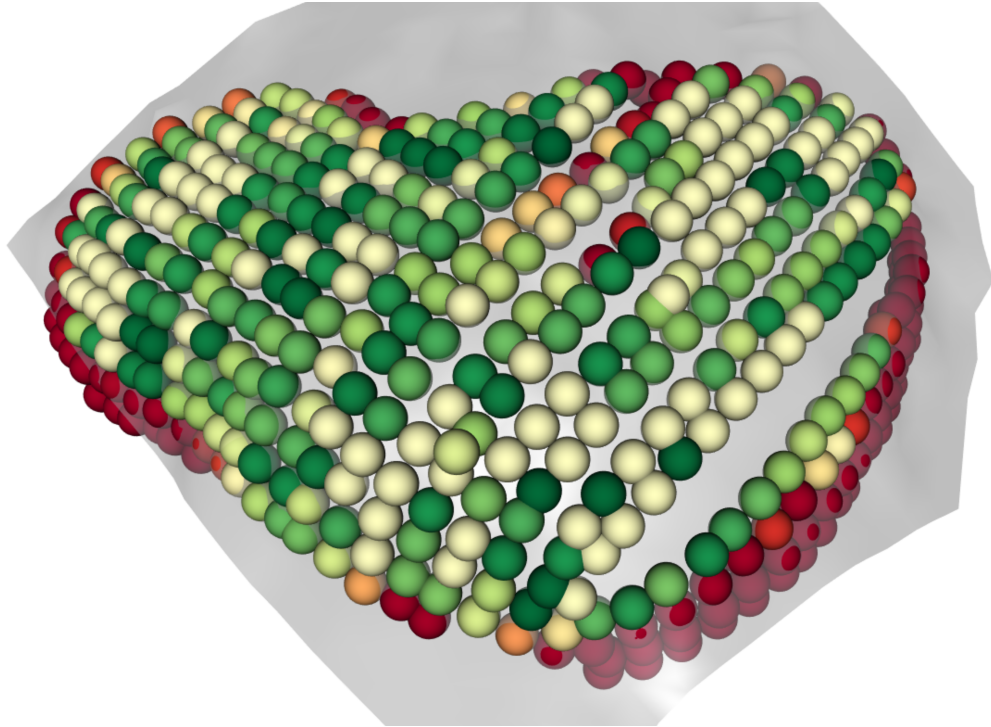


**Figure 6.5.** The mean distance of each reference point visualized by colors. All points with a mean distance of over 5 mm to the surface are colored dark red. Points with a mean distance below 1.5 mm are colored dark green.

### 6.1.3 Discussion

The surface contact detector is correctly classifying in 96% of the cases, with a very low false positive rate of 1.9%. This is especially important, as false positives lead to artifacts in the reconstructed surface. Furthermore, the processing time of 15 ms per image makes it suitable for real-time processing of the images as the ultrasound scanner runs at 20 Hz (50 ms / frame). When the US probe is removed from the liver surface there are 3-5 images which are wrongly classified as having a signal. This would cause artifacts in the surface reconstruction, and therefore they are filtered out later for surface reconstruction. This is mainly, because of the latency of the US scanner itself compared to the tracking system. The images are slightly blurrier (Figure 6.6), but from the tracking positions one can clearly see that they are not on the surface.

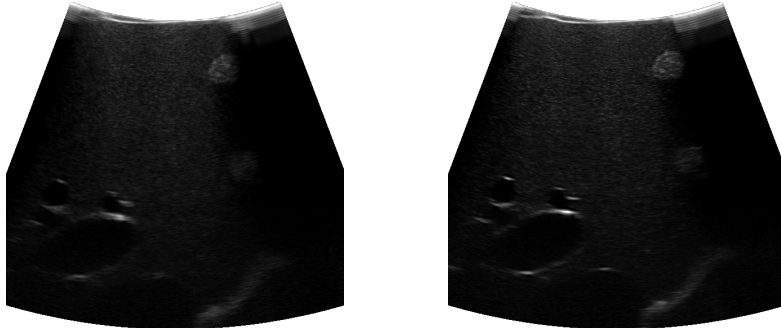


**Figure 6.6.** Wrong and correct classified images at the end of the measurement

### Surface reconstruction

From a visual point of view the reconstructed surfaces of the US liver phantom look similar to the surface of the liver model. However, the spiral and the flower movement, led to a more accurate reconstruction.

From a quantitative point of view, it turned out that the largest average errors are in segment 2 and 3. This is likely because these liver segments are the softest on the phantom used for the measurements. Due to that, this segment was pressed down during the measurement which lead to a surface with a large distance to the reference points. Additionally, one can see that the average distance at the boundary of the liver is large as well. This could be because the US device was held between the wall of the tank and the liver model. Because of the small space between the wall and the liver, the pressure applied on the liver was larger than in other areas and the consequent distance between the reference points and the deformed surface became larger. However, this might also be the case in a clinical setting, as these regions are more difficult to reach with the US probe. Overall, the best accuracy, could be achieved in segments 4,5,6 and 8, which were the easiest to access in this setup. In a next step, this would also be analyzed on the human liver, to see in which segments this technique can be applied accurately.

To conclude, we presented a surface reconstruction technique, which can be used to intraoperatively acquire a surface model of the liver using navigated US. This can then be further used for intraoperative resection planning or surface-based registration.

## 6.2 Surface reconstruction on retrospective data

### 6.2.1 Methodology

Retrospective data from Banz et. al

### 6.2.2 Results

### 6.2.3 Discussion

## 6.3 Usability Test

3 surgeons questionnaire surface accuracy (using surface registration)

6.3.1 Methodology

6.3.2 Results

6.3.3 Discussion



## Chapter 7

# Discussion and Conclusions

### 7.1 Discussion

*Interpret your results in the context of past and current studies and literature on the same topic. Attempt to explain inconsistencies or contrasting opinion. Highlight the novelty of your work. Objectively discuss the limitations.*

### 7.2 Conclusions

*Formulate clear conclusions which are supported by your research results.*



## **Chapter 8**

### **Outlook**

*Provide a vision of possible future work to continue and extend your thesis research.*



# Bibliography

- [1] Polaris Spectra and Vicra.
- [2] Surface Reconstruction Part II. Technical report.
- [3] D. Adalsteinsson and J. A. Sethian. A fast level set method for propagating interfaces. *Journal of Computational Physics*, 118(2):269–277, May 1995.
- [4] D. L. Aghayan, E. Pelanis, Å. A. Freland, A. M. Kazaryan, M. A. Sahakyan, B. I. Røsok, L. Barkhatov, B. A. Bjørnbeth, O. J. Elle, and B. Edwin. Laparoscopic parenchyma-sparing liver resection for colorectal metastases. *Radiology and oncology*, 52(1):36–41, 2018.
- [5] R. Akhtar, S. Eichhorn, and P. Mummary. Microstructure-based finite element modelling and characterisation of bovine trabecular bone. *Journal of Bionic Engineering*, 3(1):3–9, Mar. 2006.
- [6] F. A. Alvarez, R. S. Claria, S. Oggero, and E. de Santibañes. Parenchymal-sparing liver surgery in patients with colorectal carcinoma liver metastases. *World journal of gastrointestinal surgery*, 8(6):407, 2016.
- [7] E. Aulisa, S. Manservisi, R. Scardovelli, and S. Zaleski. Interface reconstruction with least-squares fit and split advection in three-dimensional cartesian geometry. *Journal of Computational Physics*, 225(2):2301–2319, Aug. 2007.
- [8] U. Bagci. MEDICAL IMAGE COMPUTING (CAP 5937) LECTURE 10: Medical Image Segmentation as an Energy Minimization Problem. Technical report, Center for Research in Computer Vision (CRCV), Florida, 2016.
- [9] V. M. Banz, P. C. Müller, P. Tinguely, D. Inderbitzin, D. Ribes, M. Peterhans, D. Candinas, and S. Weber. Intraoperative image-guided navigation system: development and applicability in 65 patients undergoing liver surgery. *Langenbeck's archives of surgery*, 401(4):495–502, 2016.
- [10] G. Baroud. High-viscosity cement significantly enhances uniformity of cement filling in vertebroplasty: An experimental model and study on cement leakage., 2006.
- [11] D. Cherqui, E. Husson, R. Hammoud, B. Malassagne, F. Stéphan, S. Bensaid, N. Rotman, and P.-L. Fagniez. Laparoscopic liver resections: a feasibility study in 30 patients. *Annals of surgery*, 232(6):753, 2000.
- [12] L.-C. Chu and C.-C. Chang. Infrared 3d scanning system, Aug. 27 2002. US Patent 6,442,419.

- [13] L. W. Clements, J. A. Collins, J. A. Weis, A. L. Simpson, T. P. Kingham, W. R. Jarnagin, and M. I. Miga. Deformation correction for image guided liver surgery: An intraoperative fidelity assessment. *Surgery*, 162(3):537–547, 2017.
- [14] L. W. Clements, J. A. Collins, Y. Wu, A. L. Simpson, W. R. Jarnagin, and M. I. Miga. Validation of model-based deformation correction in image-guided liver surgery via tracked intraoperative ultrasound: preliminary method and results. In *Medical Imaging 2015: Image-Guided Procedures, Robotic Interventions, and Modeling*, volume 9415, page 94150T. International Society for Optics and Photonics, 2015.
- [15] W. Commons. Local outlier factor, 2018. LOF.svg.
- [16] Y. Cui and D. Stricker. 3d shape scanning with a kinect. In *ACM SIGGRAPH 2011 Posters*, page 57. ACM, 2011.
- [17] M. Dou, J. Taylor, H. Fuchs, A. Fitzgibbon, and S. Izadi. 3d scanning deformable objects with a single rgbd sensor. In *Proceedings of the IEEE Conference on Computer Vision and Pattern Recognition*, pages 493–501, 2015.
- [18] J. G. D. Franca, M. A. Gazziro, A. N. Ide, and J. H. Saito. A 3d scanning system based on laser triangulation and variable field of view. In *Image Processing, 2005. ICIP 2005. IEEE International Conference on*, volume 1, pages I–425. IEEE, 2005.
- [19] D. Galun, D. Basaric, M. Zuvela, P. Bulajic, A. Bogdanovic, N. Bidzic, and M. Milicevic. Hepatocellular carcinoma: From clinical practice to evidence-based treatment protocols. *World journal of hepatology*, 7(20):2274, 2015.
- [20] H. Hoppe, T. DeRose, T. Duchamp, J. McDonald, and W. Stuetzle. *Surface reconstruction from unorganized points*, volume 26. ACM, 1992.
- [21] A. Hornung and L. Kobbelt. Robust reconstruction of watertight 3 d models from non-uniformly sampled point clouds without normal information. In *Symposium on geometry processing*, pages 41–50. Citeseer, 2006.
- [22] M. Kazhdan. Reconstruction of solid models from oriented point sets. In *Proceedings of the third Eurographics symposium on Geometry processing*, page 73. Eurographics Association, 2005.
- [23] T. P. Kingham, S. Jayaraman, L. W. Clements, M. A. Scherer, J. D. Stefansic, and W. R. Jarnagin. Evolution of image-guided liver surgery: transition from open to laparoscopic procedures. *Journal of Gastrointestinal Surgery*, 17(7):1274–1282, 2013.
- [24] T. Lange, S. Eulensteiner, M. Hünerbein, and P.-M. Schlag. Vessel-based non-rigid registration of mr/ct and 3d ultrasound for navigation in liver surgery. *Computer Aided Surgery*, 8(5):228–240, 2003.
- [25] T. Langø, S. Vijayan, A. Rethy, C. Våpenstad, O. V. Solberg, R. Mårvik, G. Johnsen, and T. N. Hernes. Navigated laparoscopic ultrasound in abdominal soft tissue surgery: technological overview and perspectives. *International journal of computer assisted radiology and surgery*, 7(4):585–599, 2012.
- [26] R. Lencioni and L. Crocetti. Local-regional treatment of hepatocellular carcinoma. *Radiology*, 262(1):43–58, 2012.

- [27] M. Levoy, K. Pulli, B. Curless, S. Rusinkiewicz, D. Koller, L. Pereira, M. Ginzton, S. Anderson, J. Davis, J. Ginsberg, et al. The digital michelangelo project: 3d scanning of large statues. In *Proceedings of the 27th annual conference on Computer graphics and interactive techniques*, pages 131–144. ACM Press/Addison-Wesley Publishing Co., 2000.
- [28] H. Li, Y. Li, R. Yu, J. Sun, and J. Kim. Surface reconstruction from unorganized points with lo gradient minimization. *Computer Vision and Image Understanding*, 169:108–118, 2018.
- [29] S. P. Lim and H. Haron. Surface reconstruction techniques: a review. *Artificial Intelligence Review*, 42(1):59–78, 2014.
- [30] A. H. Mahnken, K. E. Wilhelm, J. Ricke, et al. *CT-and MR-guided Interventions in Radiology*, volume 22. Springer, 2009.
- [31] L. Maier-Hein, A. Groch, A. Bartoli, S. Bodenstedt, G. Boissonnat, P.-L. Chang, N. Clancy, D. S. Elson, S. Haase, E. Heim, et al. Comparative validation of single-shot optical techniques for laparoscopic 3-d surface reconstruction. *IEEE transactions on medical imaging*, 33(10):1913–1930, 2014.
- [32] S. McGuire. World cancer report 2014. geneva, switzerland: World health organization, international agency for research on cancer, who press, 2015, 2016.
- [33] K. Numminen, O. Sipilä, and H. Mäkipalo. Preoperative hepatic 3d models: virtual liver resection using three-dimensional imaging technique. *European journal of radiology*, 56(2):179–184, 2005.
- [34] D. K. Pai, K. v. d. Doel, D. L. James, J. Lang, J. E. Lloyd, J. L. Richmond, and S. H. Yau. Scanning physical interaction behavior of 3d objects. In *Proceedings of the 28th annual conference on Computer graphics and interactive techniques*, pages 87–96. ACM, 2001.
- [35] M. Peterhans, S. Anderegg, P. Gaillard, T. Oliveira-Santos, and S. Weber. A fully automatic calibration framework for navigated ultrasound imaging. In *Engineering in Medicine and Biology Society (EMBC), 2010 Annual International Conference of the IEEE*, pages 1242–1245. IEEE, 2010.
- [36] M. Peterhans, A. vom Berg, B. Dagon, D. Inderbitzin, C. Baur, D. Candinas, and S. Weber. A navigation system for open liver surgery: design, workflow and first clinical applications. *The International Journal of Medical Robotics and Computer Assisted Surgery*, 7(1):7–16, 2011.
- [37] A. L. Simpson and T. P. Kingham. Current evidence in image-guided liver surgery. *Journal of Gastrointestinal Surgery*, 20(6):1265–1269, 2016.
- [38] A. K. Siriwardena, J. M. Mason, S. Mullamitha, H. C. Hancock, and S. Jegatheeswaran. Management of colorectal cancer presenting with synchronous liver metastases. *Nature reviews Clinical oncology*, 11(8):446, 2014.
- [39] S. Thompson, J. Totz, Y. Song, S. Johnsen, D. Stoyanov, S. Ourselin, K. Gurusamy, C. Schneider, B. Davidson, D. Hawkes, et al. Accuracy validation of an image guided laparoscopy system for liver resection. In *Medical Imaging 2015: Image-Guided Procedures, Robotic Interventions, and Modeling*, volume 9415, page 941509. International Society for Optics and Photonics, 2015.

- [40] G. Torzilli. Ultrasound guided liver surgery. Springer, 2014.
- [41] Wikipedia contributors. Maximum flow problem — Wikipedia, the free encyclopedia, 2018. [Online; accessed 15-October-2018].
- [42] A. D. Wiles, D. G. Thompson, and D. D. Frantz. Accuracy assessment and interpretation for optical tracking systems. In Medical Imaging 2004: Visualization, Image-Guided Procedures, and Display, volume 5367, pages 421–433. International Society for Optics and Photonics, 2004.
- [43] Y. Yu. Surface reconstruction from unorganized points using self-organizing neural networks. In IEEE Visualization, volume 99, pages 61–64. Citeseer, 1999.

*etc.*

## Appendices



## Appendix A

### Vector and Tensor Mathematics

#### A.1 Introduction

...

#### A.2 Variable Types

...



## Appendix B

### Another Appendix

B.1 Section 1

...

B.2 Section 2

...